Fast and reversible crosslinking of a silk elastin-like polymer

Constancio Gonzalez-Obeso[1,2], J.C. Rodriguez-Cabello[2], D. L. Kaplan[1]

[1]- Department of Biomedical Engineering Tufts University

4, Colby St., Medford, MA, 02155, USA

Email: david.kaplan@tufts.edu

[2]-BIOFORGE (Group for Advanced Materials and Nanobiotechnology)

University of Valladolid-CIBER-BBN

Paseo de Belén 19, 47011 - Valladolid, Spain

Email: roca@bioforge.uva.es

Abstract

Elastin-like polymers (ELPs) and their chimeric subfamily the silk elastin-like polymers (SELPs) exhibit a lower critical solvation temperature (LCST) behavior in water which has been extensively studied from theoretical, computational and experimental perspectives. The inclusion of silk domains in the backbone of the ELPs effects the molecular dynamics of the elastin-like domains in response to increased temperature above its transition temperature and confers gelation ability. This response has been studied in terms of initial and long-term changes in structures, however, intermediate transition states have been less investigated. Moreover, little is known about the effects of reversible hydration on the elastin versus silk domains in the physical crosslinks. We used spectroscopic techniques to analyze initial, intermediate and long-term states of the crosslinks in SELPs. A combination of thermoanalytical and rheological measurements demonstrated that the fast reversible rehydration of the elastin motifs adjacent to the relatively small silk domains was capable of breaking the silk physical crosslinks. This feature can be exploited to tailor the dynamics of these types of crosslinks in SELPs.

Key Words: silk, elastin, crosslinking, thermal, reversibility

Introduction

Elastin-like polymers (ELPs) are a family of stimuli-responsive proteinaceous materials based on the (VPGXG) pentapeptide found in the intrinsically disordered regions of tropoelastin [1, 2], where X stands for any amino acid but proline [3]. Their unique combination of properties, such as mechanical resilience, biocompatibility, degradability and versatility [4], thermoresponse is often exploited. ELPs exhibit a sharp lower critical solution temperature (LCST) behavior over a small window of temperatures [5], above which they spontaneously water-phase separate and self-assemble via hydrophobic interactions [6], with a fully reversible phase transition. Such thermal-reversible behavior has been extensively studied theoretically and experimentally [7-10]. Theoretical models have evolved from random-to-order phase transitions of the ELP backbone [9, 11], to the inclusion of ELPs as intrinsically disordered proteins (IDPs) [12, 13], even in the separated state in the water phase [14, 15]. The experimental and computational literature has mostly focused on measuring the effect of the X amino acid [16-18], of salts [19, 20], co-solutes [21], concentration of protein [22], molecular weight [23], co-block composition [24, 25] or tagged peptides [26] on the LCST behavior.

Silk elastin-like polymers (SELPs) are a subfamily of ELPs that retain the thermoresponsive features of the elastin-like domains but include in their structure the $(GAGAGS)_n$ motif found in *B. mori* silk fibroin. These silk domains provide the SELPs with the ability to establish robust bonds between chains, as physical crosslinks [27-29]. Silk physical crosslinking has been extensively studied using NMR [30], Raman spectroscopy [31], FTIR [32], X-Ray diffraction [33], among other methods. Briefly, uncrosslinked silk is a mixture of random coil and partially ordered structures, named silk I [34]. The ordered structures consist of small crystalline regions formed by repeated type II β-turn structures with intra- and inter-molecular hydrogen bonding. The detailed process of conversion from silk I to fully crosslinked and crystalline silk II includes dehydration and the assembly of ordered structures over different length scales [35, 36]. The

interlocking of different molecular chains into these multiscale crystals leads to robust physical crosslinking of silk as observed in fibers spun in nature by silkworms and spiders[34].

The inclusion of silk domains in the ELP backbone effects the molecular dynamics that the elastin-like domains during transitions in response to an increase in solution temperature above the LCST, as seen by circular dichroism (CD) [37], turbidimetry and dynamic light scattering (DLS) [38] and molecular simulations [39, 40], which result in different physical and mechanical properties of the macroscale protein materials [39]. The effect of silk domains on the thermoresponsive properties of the chimeric material and the effect of the reversible elastin-like LCST behavior on silk crosslinking is an understudied concept, yet critical to the design and dynamic functions of these protein systems. The effect of the uncrosslinked silk domains over the transition temperature (T_t) of adjacent elastin-like domains when compared to the same elastin-like sequence with a lower content or without silk has been reported, and results in an increase in the T_t, related to the hydrophilicity of the serines present in the silk domains [28, 40, 41]. The effect of the silk-crosslinking on the thermoresponsive behavior of the materials was also reported, but the study was limited to long (15 hours and beyond) incubation times [28], whereas intermediate states were not characterized.

Little is known about the effect of the reversible phase transitions of the elastin-like blocks in relation to the hydrogen bonding of silk motifs in SELPs. Forces involved in the rehydration of the elastin motifs are known to be significant [42, 43], whereas stable silk crosslinks in SELPs are known to develop and strengthen in aqueous solvents a time dependent manner [44-46]. We envision exploiting the fast reversible phase transition of the elastin-like motifs as a mechanism to develop temperature responsive reversible SELP hydrogels. This alternating interacting and non-interacting states can be used to switch cell-material interactions on and off [47, 48], providing temporal control of adherent cell behavior as *in vitro* models of ECM diseases [49] or other cell culture topics. Other applications include the controlled delivery of drugs and/or cells, where the thermal transition of the hydrogels can serve as a mechanism to deliver a payload on demand [50], overcoming the otherwise slow diffusion of substances.

In this work we present a time-dependent study of temperature-triggered silk-mediated physical crosslinking of a SELP, characterizing the initial, intermediate and final stages of crosslinking. We also studied how the silk physical crosslinking affects the thermoresponsive properties of the elastin domains. Finally, we demonstrate that the rapid and reversible rehydration of the elastin domains can be exploited to break the silk crosslinks.

MATERIALS AND METHODS

SELP production and characterization

Two different recombinant proteins were constructed using standard procedures. The $(VPGSG)_{25}$ sequence encoding gene was synthetized by NZYTECH (Lisbon, Portugal), cloned and dimerized in a modified pDrive vector, and subsequently ligated to the gene encoding either $(VPGIG)_{60}$ or $[(VPGIG)_{60}(GAGAGS)_{10}]$ [28]. Both structures were then dimerized, generating the SI and the SILK-SI encoding genes, and cloned into a modified version of the Pet25B expression vector (Novagen, Germany). The recombinant proteins were expressed in *E. coli* BLR(D3) (Stratagene, USA), grown in TerrificBroth (Foremedium, Norfolk, UK) and purified by taking advantage of their thermoresponsive properties [51]. The proteins were dialyzed against ultra-pure water and freeze-dried. Purity and composition were assessed by 10% SDS-PAGE, matrix assisted laser desorption/ionization time-of-flight mass spectrometry (MALDI-TOF) (Bruker Autoflex, Billerica, Massachusetts, USA), amino acid analysis, deuterated DMSO solution proton nuclear magnetic resonance (H-NMR) (Bruker RMN 400Hz, Billerica, Massachusetts, USA) and amino acid analysis (6M HCl 1% phenol digestion, followed by High Performance Liquid Chromatography) [44, 52, 53]. The detailed characterization is reported in the Supporting Information.

Rheology

Mechanical properties were measured using freshly prepared 100 mg/mL solutions in PBS and an oscillatory rheometer (TA Instruments AR2000ex, New Castle, Delaware, USA) equipped

with a Peltier for temperature control using a 25 mm flat geometry, 0.5% of strain and a frequency of 6.28 rad/s, within the linear viscoelastic conditions of the material (see Supporting Information). Samples were heated from 1 to 37ºC at 2.5ºC/min and subsequently maintained at 37ºC for another 45 minutes. In order to avoid dehydration artifacts due to the experimental temperatures and long-term experiments, the samples were analyzed inside a specially-design chamber that avoids solvent evaporation. Mechanical properties of the formic acid treated SILK-SI samples dissolved in PBS at 100 mg/mL and subjected to the same thermal treatment are shown in the Supporting Information.

Spectroscopy of crosslinking

Spectroscopic analysis of the proteins (FTIR, FT-Raman and X-Ray diffraction) was performed using a 100 mg/mL solution in PBS. For each time point (180 min for the SI control; 5, 30 and 180 minutes, and 12 hours for the SILK-SI), samples (200 µL each) were poured into hermetically sealed, flat–bottom vials and incubated at 37ºC. Subsequently, the samples were immersed in liquid nitrogen and lyophilized. To achieve the least crosslinked sample, SILK-SI was dissolved in formic acid (FA) for 24 hours, dialyzed against ultrapure water at 4ºC and lyophilized. FA treated samples were prepared in the same way, but only heated at 37ºC for 30 seconds, enough for the isoleucine domains to phase transition [45]. In this way, the changes in the FA treated samples and the rest of the SILK-SI samples could be attributed to the silk crosslinking.

FTIR

Samples were analyzed by attenuated total reflectance Fourier transform infrared spectroscopy (ATR-FTIR) (Bruker Tensor27, Billerica, Massachusetts, USA, 512 scans, 1 cm^{-1} resolution). Amide I peak analysis and deconvolution were performed with PeakFit v4.12 (Systat Software Inc.) by fitting the experimental data with Gaussian curves [32, 35, 54].

FT-Raman

Fourier transform Raman spectra were acquired with a MultiRAM Stand Alone FT-Raman Spectrometer (Bruker, Billerica, Massachusetts, USA), equipped with a Nd:YAG laser centered

at 1064 nm. For analysis, 400 scans were performed with a resolution of 2 cm^{-1}. Prior to the analysis, spectra were normalized to methylene bending at 1450 cm^{-1}, which is insensitive to changes in secondary structure [55]. Bands for silk I and silk II were assigned according to the literature [55-58].

X-Ray diffraction

The X-Ray diffraction patterns, with 2Θ ranging from 6 to 40º, were collected in a XPert XRD (Philips, Eindohoven, The Netherlands) equipped with a high intensity ceramic sealed tube as the X-Ray source (3kW) and Cu K-α (with an energy of 8.04 keV and a wavelength of 1.54 Å). Samples were placed inside a polyethylene terephthalate foil, needed for holding sample in place. Experiments were performed in transmission mode.

For the FTIR, Raman and X-Ray spectroscopic techniques, samples were immersed in liquid nitrogen and cryo-fractured prior to lyophilization. For FTIR and Raman special care was taken to analyze the core rather than surface of the samples to avoid artifacts related to sample manipulation or surface-induced changes.

Thermal analysis of SELPs

Differential scanning calorimetry (DSC) experiments were carried out in a Mettler Toledo DSC822e (Columbus, Ohio, USA) using hermetically sealed aluminum pans. For each sample, a volume of 20 µL (100 mg/mL solution in PBS, pH 7) was used, with an equal volume of PBS as the reference. Samples were subjected to 20 temperature cycles (5 minutes isotherm at 1ºC, heating ramp up to 30ºC, 5 minutes isotherm at 30ºC and a cooling ramp down to 1ºC; temperature ramps were performed at 2.5ºC/min). The SILK-SI sample and its reference were then incubated for 12 hours at 37ºC and subjected to other 6 thermal cycles. The SI sample (100 mg/mL in PBS) was subjected to 6 complete thermal cycles. Formic acid treated SILK-SI samples were subjected to 10 complete thermal cycles, incubated for 12 hours at 37ºC and subsequently subjected to another 4 thermal cycles (Data shown in Supporting Information).

Statistical Analysis

Otherwise stated, all measurements were performed in triplicate. Presented values are the average and errors represent the standard deviation of those measurements.

RESULTS

SELP production and characterization

The amino acid sequences and molecular weight of both polymers, with and without silk (SILK-SI and SI, respectively) are summarized in Table 1. The proteins were purified by taking advantage of their thermoresponsive nature, as seen by SDS-PAGE (Supplemental Figure 1), MALDI-TOF (Supplemental Figure 2) and H-NMR (Supplemental Figure 3). Both yielded at least 350 mg of pure protein per liter of cultured bacteria. The amino acid composition was assessed by amino acid analysis (Supplemental Table 1), and DSC was used to assess thermoresponsive features and the corresponding T_t: 15.7 and 16.8ºC for the SI and the SILK-SI polymer, respectively (Supplemental Figure 4).

Table 1. Name, amino acid sequence ant theoretical molecular weight of the two polymers, the elastin with silk (SILK-SI) and without (SI).

NAME	Amino acid sequence	Theoretical MW (kDa)
SILK-SI	MESLLP-$[(VPGSG)_{50}$-$(VGIPG)_{60}$-$(GAGAGS)_{10}]_2$-V	99.36
SI	MESLLP-$[(VPGSG)_{50}$-$(VGIPG)_{60}]_2$-V	91.35

Rheology

Rheological measurements for both proteins revealed different behavior (Figure 1). The SILK-SI remained as a solution (G''≥G'≈1-3 Pa) up to 16.8ºC, in agreement with the T_t measured by DSC. Above this temperature, the elastic and loss moduli sharply increased. At 20.5ºC, the solution gelled (G'=G''=541.7 Pa, tg(δ)=1). Upon gelation the elastic modulus continued to increase up

to 883.5 Pa to then decrease down to values around 600 Pa and plateau, whereas loss modulus decreased down to 200 Pa and plateaued. After 40 minutes (26 minutes of incubation at 37ºC) both G' and G'' grew in parallel and reached a plateau of 5.1 and 1.2 kPa, respectively. The SI polymer exhibited slightly lower mechanical properties than the SILK-SI (G''≥G'≈0.1-05 Pa) up to 15.9ºC, very close to the T_t measured by DSC. Above this temperature they decreased to G'≈G''≈0.04 Pa.

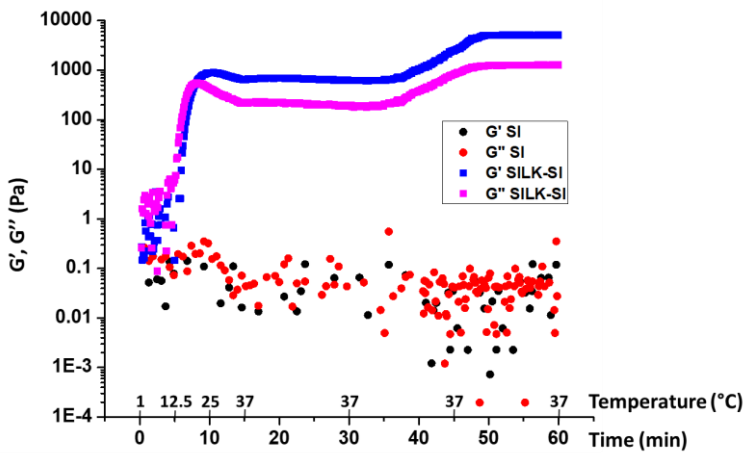

Figure 1. Elastic (G') and loss (G'') moduli for the SILK-SI and the SI proteins. The two proteins exhibited differences, with the SILK-SI forming a stable hydrogel in response to a temperature increase above its T_t (16.8ºC) and further stiffening with increased incubation time. In contrast, the SI polymer exhibited weak mechanical properties which, decreased as the temperature increased.

Fourier Transform Raman spectroscopy

In the Fourier transform Raman spectra the FA treated SILK-SI and SI polymer exhibit similar, wide and less defined, spectra, showing typical Raman peaks for elastin-like polymers (Figure 2) [59]. For the SILK-SI samples, even after 5 minutes the spectra show more defined peaks, with clear signals related to silk I (856, 1102 and 1245 cm^{-1}) and silk II (876, 973, 1085 and 1228 cm^{-1}) crystals. Such signals become sharper with longer incubation times at 37ºC. The amide I band shifted from a maximum of 1672 to 1665 cm^{-1} with time.

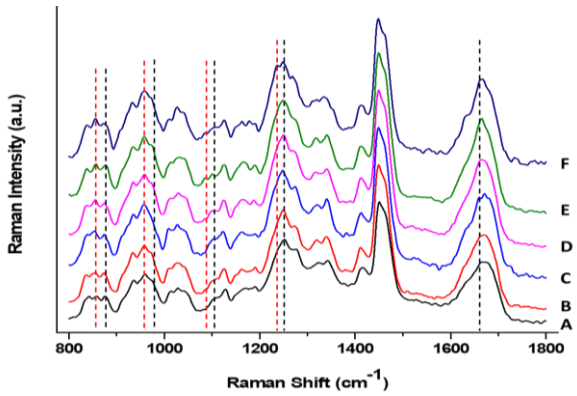

Figure 2. Fourier transform Raman spectra (range 800-1800 cm^{-1}) for: (A) FA treated SILK-SI, (B) 180 minutes incubated SI, (C) 5, (D) 30 and (E) 180 minutes incubated SILK-SI; and (F) for the 12 hour incubated SILK-SI. Longer incubation times revealed sharper silk I (red dashed lines) and silk II (black dashed lines) signals.

FTIR amide I peak analysis

The FTIR amide I peak and its deconvolution for each sample is in Figure 3. Amide I peak maxima consistently shifted towards lower wavelengths, from 1629.8 cm^{-1} for the FA SILK-SI sample to 1619.9 cm^{-1} for the 12 hours 37ºC incubated SILK-SI sample. The other samples peaked between these two values: 1628.4 cm^{-1} for the SI sample; 1625.7, 1621.6 and 1620.6 cm^{-1} for the SILK-SI samples incubated 5, 30 and 180 minutes, respectively (Figure 3 A to F). The amide I peak was deconvoluted and the contribution of side chain, β-sheet, random coil, α-helix and β-turns are shown in Figure 3G. The data show a consistent change in the signals except for the FA treated and the SI samples, whose analyses revealed similar contributions. For the rest of the SILK-SI samples, side chain and β-sheet signals increased from 3.6 to 7.1% and 39.3 to 48%, respectively; while beta turn and "random coil + alpha helix" signals decreased from 41.2 to 31.2% and 15.7 to 13.5%, respectively.

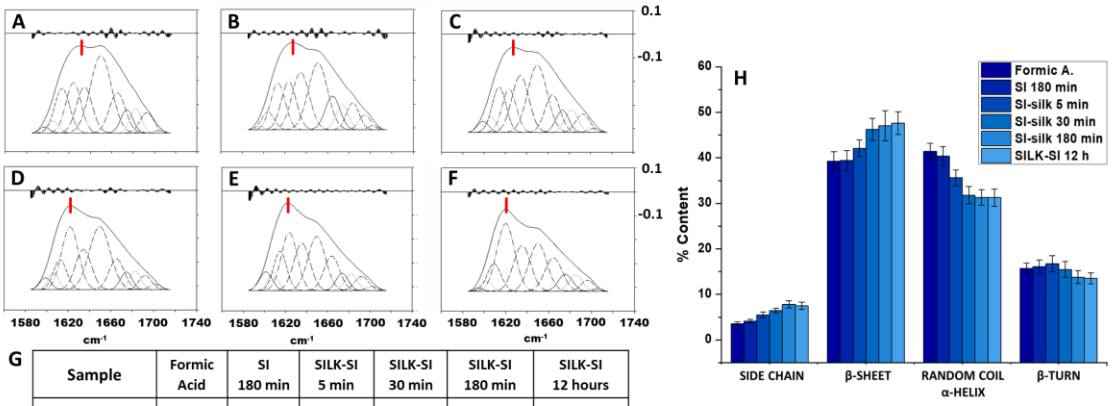

G

Sample	Formic Acid	SI 180 min	SILK-SI 5 min	SILK-SI 30 min	SILK-SI 180 min	SILK-SI 12 hours
Amide I peak maxima (cm^{-1})	1629.8	1628.4	1625.7	1621.6	1620.6	1619.9

Figure 3. Deconvolution of the FTIR amide I peak of the: (A) FA treated SILK-SI, (B) 180 minutes incubation SI, (C) 5, (D) 30 and (E) 180 minutes incubation SILK-SI and (F) the 12 hour incubation SILK-SI sample. Maxima are indicated with a red mark. Residuals are shown above the deconvolutions. (G) Displacement amide I peak maxima towards lower wavelength as a function of sample treatment. (H) The contribution, expressed as percentage, of each signal (side chain, beta-sheet, random coil + alpha-helix and beta-turn) to the amide I peak.

X-Ray diffraction

X-Ray diffractograms of SI and SILK-SI samples are shown in Figure 4. The SI sample incubated for 180 minutes and the FA treated SILK-SI sample exhibit, both, a similar wide halo. The peak at $2\Theta=16^{o}$ is an experimental artifact from the sample holder. For the SILK-SI samples, the longer the incubation time the more the diffraction peaks increased at characteristic angles of silk I ($2\Theta=20.3^{o}$ and 24.6^{o}) and silk II ($2\Theta=19.8^{o}$ and 24.8^{o}). For the 12-hour incubated sample, previous signals increased and developed clear diffraction peaks and new, sharp signals appear at $2\Theta=8.9^{o}$ and 18.2^{o} for silk I and $2\Theta=12.2^{o}$ for silk II. The signals were assigned based on the information in the literature [60-62].

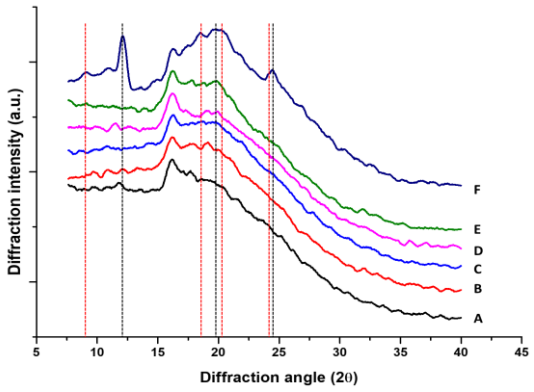

Figure 4. X-Ray diffraction patterns of the: (A) SI incubated 180 minutes, (B) the SILK-SI sample treated with FA, the SILK-SI sample incubated for: (C) 5, (D) 30 and (E) 180 minutes; and (F) SILK-SI sample incubated 12 hours. Samples exhibited a consistent increase in signal intensity related to the formation of silk I (red dashed line) and silk II (black dashed line) crystal motifs.

Heating-Cooling Thermal analysis of SELP

The SILK-SI was subjected to 26 heating and cooling cycles with the thermograms shown in Figure 5A, with the complete runs in the Supporting Information. The thermogram of the first heating cycle for the SILK-SI shows a unique transition peak at 16.75°C (Figure 5A). In the second heating cycle, this signal shifted towards a higher temperature with a lower intensity, and a new shoulder appeared at lower temperatures (12.458°C). As the number of cycles increased, the peak maximum in the first heating cycle continued to displace towards higher temperature (reaching up to 17.7º C) and reduced in intensity, becoming a slight shoulder after cycle 9; the shoulder found upon the second heating cycle at 12.5ºC increased in intensity while the maximum remained constant.

Thermograms of the cooling cycles follow a similar trend (Figure 5A), although some differences were found. The first cooling cycle already showed a double phase transition, composed of a dominant peak at 16.0ºC and a shoulder at 11.2º C. In subsequent cooling cycles, the main peak maximum in the first cycle shifted towards higher temperature (reaching up to 16.8ºC) and decreased in intensity, disappearing after the 11th cycle. In contrast, the shoulder at 11.2 ºC

increased in intensity while maintaining the same maximum. Thermograms of the 6 heating and cooling cycles of the SILK-SI after 12 hours incubation at 37ºC showed little differences.

The SI sample was subjected to 6 heating and cooling cycles (Supporting Information). The thermograms exhibited totally reversible phase transitions, where only one peak was found in both the heating and the cooling cycles at 15.6±0.1ºC and 14.6±0.1ºC, respectively (Figure 5B).

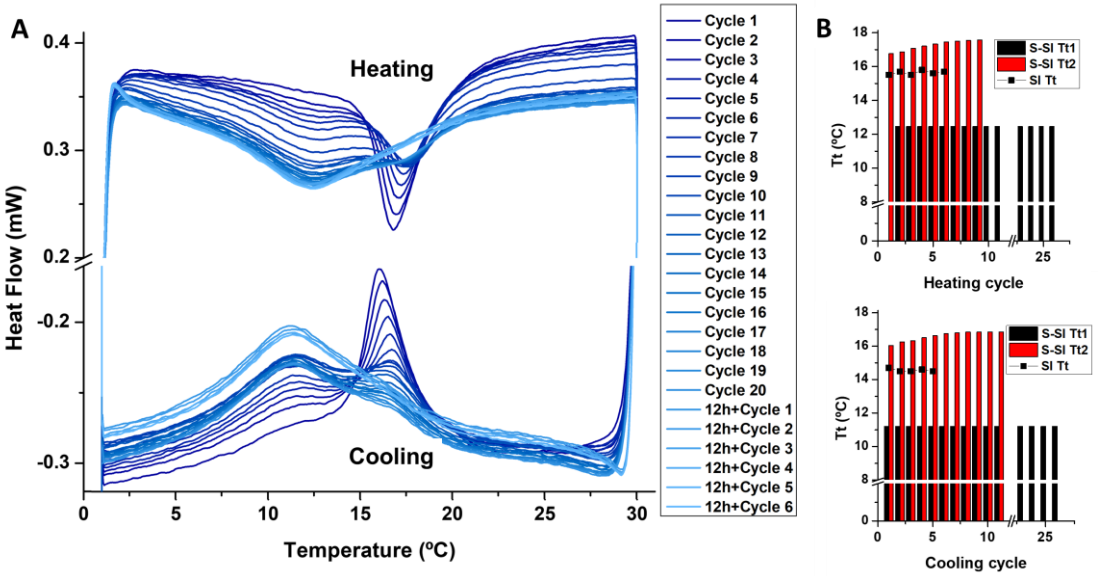

Figure 5. (A) Details of thermograms for the heating and cooling of a 100 mg/mL SILK-SI solution in PBS, showing a smooth evolution of the endotherms as the number of cycles increased. (B) The evolution of the T_t observed for both signals (16.75ºC, red columns; 11.2ºC, black columns) along 26 heating and cooling cycles. Black dots represent the T_t observed for the SI along 6 heating/cooling cycles.

Heating-Colling Rheological analysis of SELP

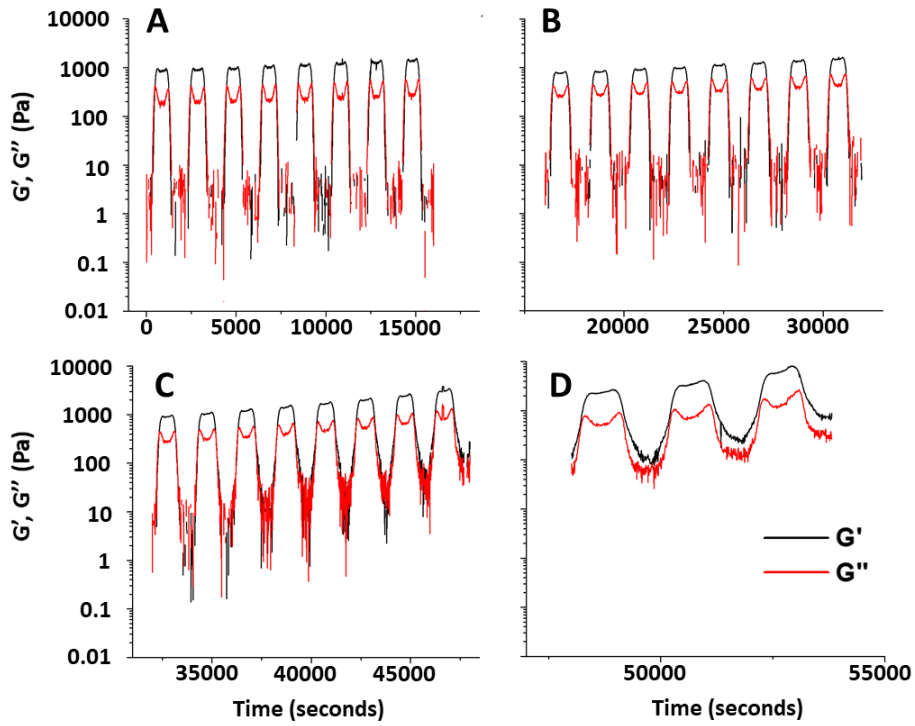

Figure 6. Evolution of the mechanical properties of the SILK-SI as function of thermal input. (A) Shows the first 8 heating and cooling cycles, (B) cycle from 9 to 17, (C) cycle from 18 to 24 and (D) last 3 cycles.

The SILK-SI shows similar results to those obtained in the first rheological experiment (Figure 1) along the first cold isotherm (1ºC) and heating stages (heating ramp and isotherm at 30ºC). Along the first cold isotherm, the SILK-SI remained water soluble and exhibited weak mechanical properties (G''≥G'≈1-3 Pa). In the first heating, once the temperature rose above the T_t of the SILK-SI, the mechanical properties rapidly increased and gelled at around 17ºC (G'=G''=493.8Pa). The elastic modulus increased as the temperature continued to increase (Figure 6, segment B) reaching values of 1.05 kPa, whereas its loss modulus decreased down to 180 Pa. During the first isotherm at 30ºC the mechanical properties were virtually constant.

At the initiation of the first cooling stage, the mechanical properties of the SILK-SI slightly increased but, as soon as the SILK-SI sample was cooled below its Tt, the properties decreased to G''≥G'≈1-5 Pa and remained in this range all along the second cold isotherm.

In the second cycle, along the heating stage, once the temperature rose above the Tt, the mechanical properties rapidly increased and reached slightly higher values at the end of this stage than at the end of the first heating stage for elastic and loss moduli. In the second hot isotherm, similar to the first, the mechanical properties again slightly increased and reached higher values for both moduli than in the first hot isotherm. In the second cooling stage, the mechanical properties dropped significantly once the temperature reaches values below the T_t for of the SILK-SI and remained similar to those found in the previous cooling stage.

This behavior was repeated in each of the 27 cycles where the mechanical properties increased during the heating stage and grew further during the hot isotherm, reaching higher values at the end of both stages than those at the end of the same stage in the previous cycle. Whereas mechanical properties decreased in the cooling stages and were further reduced during the cold isotherm, they remained higher than those found at the end of the same stage in the previous cycle. This behavior was more markedly upon the 17^{th} cycle, were differences within successive cycles and between the start and the end of the same cycle are more notorious. After cycle 23 the SELP remained as an hydrogel even in the cooling stages, as seen by the greater value of G' when compared to G''.

DISCUSSION

Rheology

Despite the similar features of SI to other ELRs capable of physically crosslinking [28], this protein did not form a hydrogel with increased temperature. Instead, the mechanical properties decreased as the temperature rose above 15.9ºC (temperature at which the phase transition takes place, by DSC). This thermal behavior was related to hydrophobic folding and association of isoleucine domains (IB). Even at a high concentration (100 mg/mL), the SI molecules were not capable of entangling among the different hydrophobic clusters formed by the phase transitioned IB [63-65], but seem to aggregate into independent nanometer sized particles (31.54 nm, PdI:

0.266), as seen by DLS (See Supporting Information). The absence of cohesiveness between SI particles seems reasonable due to the lack of interacting groups that would otherwise foster inter-particle interactions and the small repulsion between surface exposed polar residues in the N-terminal of the SI (Z-Pot of -5.18±2.23 mV). The second decrease in mechanical properties at 31ºC could be due to further reorganization of the SI molecules into smaller particles (See supporting information), as result of a closer interactions among the isoleucine hydrophobic cores, which results in a reduction of the volume fraction of the colloid suspension, and thus, a reduction in the already limited mechanical properties [66].

The SILK-SI exhibited different behavior when compared to the SI polymer due to the presence of the silk domains. The initial higher mechanical properties found at temperatures below the Tt were attributed to the few silk crosslinks that might be formed during purification of the polymer [52]. The sharp increase in mechanical properties above the T_t was related via ultra-fast silk crosslinking induced by the increased local concentration derived from the hydrophobic associations of IB. As IB associated into hydrophobic clusters, the silk motifs were carried along (Figure 7C), increasing local concentration and facilitating the nucleation of silk crystals that grew and incorporated more silk motifs to crosslink the SILK-SI. The slight decrease in both, the elastic and loss moduli were attributed to the reorganization of the isoleucine motifs as result of an increase in temperature, as observed in the SI polymer. The parallel plateau and subsequent growth of G' and G'' seemed reasonable regarding the molecular structure of the SILK-SI. The crosslinking of the SILK-SI involved locking a visco-elastic spring from both sides (Figure 7B); the silk motifs as the locks and the visco-elastic spring as the elastin-like blocks. The greater the number of linked silk motifs, the more visco-elastic chain crosslinks, and thus, further contribution to the loss and elastic moduli. After 26 min of incubation at 37ºC, both moduli reach a plateau value, indicating that all possible silk crosslinks had formed.

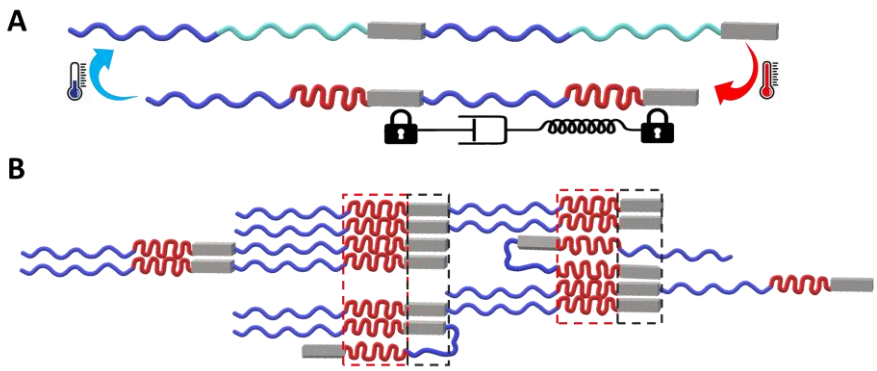

Figure 7. (A) Schematic of the SILK-SI below the T_t and above the T_t. Silk domains (gray boxes) are labelled in with a lock, representing the interlocking chains, while the elastin domains (blue: serine domain, red: phase transitioned isoleucine domain) are identified with the viscoelastic properties of the material. (C) Schematic on how the hydrophobic interactions (red dashed boxes) of the isoleucine elastin domains bring together the silk domains (black dashed boxes), facilitating crystallization.

Fourier Transform Raman spectroscopy

The sharper and more defined spectra for the SILK-SI samples incubated at 37ºC, in comparison with that of the SI and the FA treated SILK-SI, revealed a more ordered and defined structure. The similarity between the FA-treated sample and the SI sample revealed the effectiveness of the FA treatment in removing crosslinks that may have occurred during purification of the protein [67]. Further, the 30 seconds of incubation at 37ºC was sufficient for the IB of the SILK-SI polymer to completely phase transition from water-soluble to water-insoluble [68, 69]. The spectra showed that a short incubation time (5 minutes) was sufficient for the formation of silk crosslinks, based on the appearance of silk I and silk II related peaks. Longer incubation times increased the amount and intensity of silk I and silk II signals, consistent with the formation of more silk crystals of different sizes (i.e., crosslink regions), as well as a consistent shift in the maximum of the amide I band, as an indicator of the formation of silk II [70, 71]. Such results were similar to those observed with the rheological measurements, where longer incubation times

above the T_t of the SILK-SI resulted in higher mechanical properties as result of the increased crosslinks.

FTIR analysis

The consistent shift of the SILK-SI amide I peak towards lower wavelengths with increased incubation time indicated the formation of silk crosslinks [54]. Even for the shortest incubation time (5 minutes) there was clear displacement of the maximum amide I peak, supporting the formation of silk crosslinks. Displacement of amide I peak towards lower wavelengths was related to the decrease in random coil and increase in β-sheet content. Such behavior was clearer with the amide I deconvolution analysis (Figure 3G). As with the Raman spectroscopy, the FA-treated SILK-SI and the SI samples revealed similar spectra and the lowest content of β-sheet and highest content of random coil and α-helix, as a result of the acid treatment [72] for the SILK-SI and the absence of the silk domains in the SI control.

For the SILK-SI samples we observed a consistent increase in β-sheet content, while random coil and α-helix signals decreased. Both changes were consistent with the transition of the silk motifs from random coil in the un-crosslinked state to organized beta-sheets [73]. After 30 min of incubation, both, β-sheet and random-coil signals changed slightly with longer incubation times, consistent with the rheological measurements, where mechanical properties plateaued 34 minutes after the temperature surpassed the T_t of the SILK-SI. Interestingly, both side chains and β-turn signals consistently changed with incubation time, increasing and decreasing, respectively. Crosslinked silk motifs adopted either a parallel or antiparallel beta-sheet structure with about 4Å distance between adjacent sheets [74]. This close packing of the silk motifs seems to distort the adjacent phase transitioned IB, reducing the amount of β-turn content in its vicinity. The reduction in these β-turns is consistent with increased side chain signal, as the amino acid side chains in these distorted β-turns were less packed with more mobility [9].

X-Ray diffraction

The SI and SILK-SI treated with FA revealed similar X-Ray diffraction patterns characteristic of non-crystalline materials. The longer the incubation time for the SILK-SI sample the more prominent the peaks related to silk crosslinks (silk I and silk II), consistent with the Raman and FTIR amide I analyses. The sharp peaks observed at 12 hours do not reflect an increase in number of silk I and silk II crystals. In the rheology, mechanical properties plateaued after 34 minutes above the T_t for the SILK-SI, whereas in FTIR β-sheet formation was similar after 30 minutes of incubation above the Tt. Thus, the sharp increase in silk I and silk II signals was related more to alignment of already crosslinked silk motifs, which does not increase the mechanical properties but increases diffraction of these structures, revealing the sharper X-Ray diffraction signals [75-79].

Heating-Colling Thermal analysis of SELP

Previous techniques have shown rapid crosslinking of the silk domains. For example, rheological measurements showed that as soon as temperature is above the T_t for SILK-SI, crosslinking begins. In addition, the crosslinking process in silk elastin-like polymers induces changes in thermoresponsive properties [28]. While the temperature is above the T_t, the IB interact as hydrophobic entities, fostering hydrogen bonding among the silk domains, as demonstrated with rheological measurements. If the temperature is below the T_t, IB are water-soluble again, and rehydrate by water clathrate formation. The H-bonding interactions among crosslinked silk domains influences the capacity of these IB to interact with water for solvation [28]. These facts prompted us to perform time-course thermoanalytical analysis of the SILK-SI to understand how physical crosslinking of the silk domains affects the thermal properties.

The samples were subjected to 26 cycles of 4ºC isotherm-heating ramp-30ºC isotherm-cooling ramp (Figure 8A**¡Error! No se encuentra el origen de la referencia.**). The first isotherm at 4ºC ensured complete solubility of the SILK-SI before the heat ramp, while in subsequent cycles this temperature permitted the rehydration of the isoleucine motifs. The heat ramp served to support the analysis of the thermal behavior of the samples after cooling at 4ºC, while the cooling ramp served supported the analysis of the samples after heating at 30º C.

All of the phase transitions were related to the IB, as they are the only elastin domain that phase transitions in the temperature range studied [18, 80]. The single peak observed in the first heating cycle indicated a single population of phase transitioning IB. The existence of a double phase transition in the first cooling cycle (after 5 minutes of incubation at 30ºC) indicated the presence of two populations of phase-transitioning IB. The peak at 16ºC was related to the phase transition of uncrosslinked IB (U-IB), which suffered typical hysteresis towards lower T_t when compared to the heating cycle [81, 82]. In contrast, the shoulder at 11.2ºC related to the silk-crosslinked IB (C-IB), as the silk crosslinks lower the T_t of the nearby elastin domains [28]. Five minutes at 30ºC (above the T_t) was sufficient to form effective silk crosslinks, based on the rheology and spectroscopic results.

In the second heating cycle revealed a double phase transition composed of a main peak at 16.8ºC, 0.2ºC higher and lower intensity than in the first cycle. This also included a less intense shoulder than that observed in the first cooling cycle, at 12.5ºC. The peak was related to the U-IB and the shoulder to the C-IB. The decrease in the intensity of this shoulder, when compared to the first cooling cycle, revealed a reduction in the number of IB that phase transition at this temperature (C-IB). Further heating cycles shifted the peak maxima towards higher temperatures, while decreasing the intensity and disappearance after the ninth cycle. In contrast, the shoulder signal consistently increased in intensity, becoming a defined peak above the fifth cycle, and maintaining maxima constant.

The second and subsequent cooling cycles followed a similar trend as the heating cycles, while some subtle differences were found. The main peak found in the first cooling cycle (related to the U-IB) systematically shifted towards lower T_t and decreased in intensity, disappearing after the eleventh cycle. The shoulder found at 11.2ºC increased in intensity and became a clear peak after the third cooling cycle. Interestingly, the shoulder found at lower temperatures increased with cooling cycles, when compared to the same heating cycle. Such behavior was related to the transformation of the U-IB population into a C-IB population. The increase in the C-IB population at the expense of U-IB was responsible for the increase in intensity of the shoulder found at

12.5ºC. The decrease in the number of U-IB, was responsible for the displacement towards higher temperatures (as the concentration of this population decreases [23]) and the decrease in intensity of the peak found in the first heating cycle. Although the C-IB population increased with each heating cycle, the T_t did not shift towards lower temperature. This effect was explained due to the fact that the reduction of the T_t of these domains was related to the crosslinking of adjacent silk domains.

There are two remarkable facts in the thermal behavior of the SILK-SI that point out a previously unobserved effect. The first fact is that the disappearance of the signal related to the U-IB in the heating and cooling stages takes place at different cycles, disappearing in the ninth cycle for the heating and in the eleventh cycle for the cooling stage. Second, the fact that the shoulder related to the C-IB became clearer in the heating and cooling stages, also at different cycle numbers (fourth and second, respectively). These two facts suggest that during the cooling isotherms, the rehydration of the IB can disrupt some of the previously formed silk crosslinks (Figure 8), decreasing the population of C-IB and increasing that of the U-IB. Thus, the rapid rehydration of the elastin domains in the SELPs studied here, located adjacent to the relatively small silk domains, appears capable of disrupting previously formed silk physical crosslinks, when these silk domains are relatively small in size.

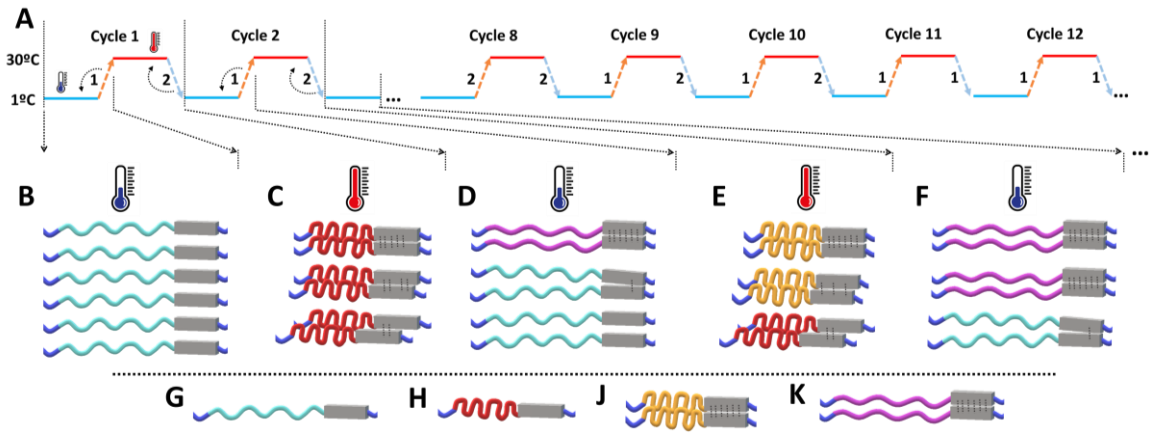

Figure 8. (A) Schematic of the DSC thermal program for the SILK-SI samples. Blue and red line stand for the cold and hot isotherms (4 and 30ºC), respectively, whereas the dashed red and blue

arrows stand for the heating and cooling ramps, respectively. Numbers shown represent the number of transitions found at each heating/cooling ramp. (B-F) Schematic of the thermal behavior of the IB and the proposed mechanism of formation and breakdown of silk crosslinks due to the reversible phase transition of the IB along the first two and a half cycles. (B) After the first isotherm at 4ºC all IBs are hydrated. (C) As temperature rises above the T_t, all IB phase transition at the same T_t and the hydrophobic interactions facilitate H-bonding between silk motifs. (D) Lowering the temperature below the T_t permits the rehydration of the Ibs. Lightly bound silk motifs are broken due to the rehydration of the adjacent IB, whereas tightly bounded silk motifs remain crosslinked, which changes the thermal properties of the adjacent IB. Successive heating stages € increase both the number and strength of silk crosslinks, increasing the number of C-IB at the expense of U-IB, whereas hydration of IB in the cooling stages (F) is capable of breaking some lightly bound silk crosslinks. Schematic of the hydrated U-IB (G), the phase transitioned U-IB (H), phase transitioned C-IB (J) and hydrated C-IB (K).

The behavior of the SI control was typical of an ELP [83], and very different from the SILK-SI. With six thermal cycles a complete reversible phase transition with a small hysteresis of about 1ºC was observed. The different thermal behavior was attributed to the silk domains as the difference among both constructs.

Heating-Cooling Rheological analysis of SELP

In order to corroborate the results obtained in the heating-cooling thermal analysis of the SILK-SI, the sample was subjected to the same heating-cooling program while the mechanical properties were measured. The similarity of results between the first rheological experiments and the first three stages (cold isotherm, heating ramp and hot isotherm) indicated the reproducibility of the results. When the temperature remained below the T_t for the SILK-SI, the mechanical properties remain low, corresponding to the water soluble state of the polymer. When the temperature rose above the Tt, the IB sharp phase transition to a water-insoluble state allowed the

adjacent silk domains to interact and crosslink. As result of this crosslinking, the mechanical properties increased and continued to do so along the first hot isotherm as further crosslinks formed with the silk domains.

This phenomenon continues to the initial stages of the first cooling ramp, as the temperature remains above the T_t. As soon as the temperature was below the T_t of the SILK-SI, the mechanical properties dropped due to the rapid reversible phase transition of the IB into the soluble form. In this transition the IB lost their characteristic molecular conformation responsible for the elastic properties and adopted a random conformation.

Interestingly, even though IB phase transitioned and became water soluble in the previous cooling ramp, the mechanical properties continued to decrease along the second cold isotherm (being this phenomenon much clear in the last 3 cycles). This loss in mechanical properties can be explained if the rehydration of the IB can break some of the previously formed silk crosslinks. The forces that drive this rapid rehydration of the elastin motifs are strong [42, 43, 84-87] and are directed perpendicular to the stacking direction of the silk motifs [88, 89]. Reduced efficiency of H-bonding or poor chain registry can be issues involved [90] (Figure 8). This hypothesis is supported by the DSC analysis, were signals related to C-IB disappeared, or become weaker, after cooling the sample below its T_t (Figure 5).

In successive temperature cycles, the mechanical properties increased as the temperature rose above the T_t, reaching higher values than in the same stage of the cycle immediately before, due to the phase transition of both the C-IB and U-IB, which recover their elastic properties and to the increasing number of silk crosslinks. The mechanical properties decreased as the temperature was lowered below the Tt, for the same reasons as in the first cycle, but remained higher than at the end of the same stage of the previous cycle due to the increased number of stable silk crosslinks formed in the warmer stages.

Conclusions

Two recombinant proteins, SILK-SI and SI, were designed and biosynthesized, differing in the presence of *B. mori* silk fibroin derived domains. Both proteins were thermoresponsive with the small differences measured in the T_t attributed to the increased hydrophilicity the silk motifs with surrounding phase transitioning isoleucine domains [26, 28]. The fast gelation of SILK-SI was related to the crosslinking of the silk domains, as the SI did not form hydrogels in response to an increase in temperature. Instead, the SI formed nanometer sized nanoparticles, as seen by DLS. Spectroscopic analysis (Raman, FTIR, X-Ray diffraction) revealed that 5 minutes of incubation above the T_t was sufficient for the SILK-SI to form stable silk crosslinks and 30 minutes of incubation above the T_t was sufficient for most silk domains to crosslink. These results were corroborated by rheology, as mechanical properties plateaued after 34 minutes above the T_t of the SILK-SI. The heating-cooling thermal and rheological analysis of the SILK-SI confirmed that 5 minutes was sufficient for the silk domains to crosslink, based on the increase in mechanical properties and the appearance of a second population of phase transitioning IBs at lower temperatures via DSC, associated to the C-IB. As the number of thermal cycles increased the intensity of the DSC signal related to the C-IB increased, indicating the formation of new silk crosslinks. The forces involved in the rapid rehydration of the IBs in the cooling stages were responsible of the reversal of silk crosslinks, as seen by the lower intensity of the DSC signals related to the C-IB after the cooling stage and the decrease in the mechanical properties when the temperature was below the T_t based on rheology. The reversible rehydration of the elastin-like blocks in a SELP can result in the breaking of the H-bonding responsible for the silk crosslinks when these domains are relatively small.

Acknowledgements

We thank the NIH (P41EB027062) and the ARO (W911NF-17-1-0384) for support of these studies. JCRC is grateful for the funding from the Spanish Government (PID2019-110709RB-100, RED2018-102417-T), Junta de Castilla y León (VA317P18, Infrared2018-UVA06), Interreg

V España Portugal POCTEP (0624_2IQBIONEURO_6_E) and Centro en Red de Medicina Regenerativa y Terapia Celular de Castilla y León.

References:

[1] Tarakanova A, Yeo GC, Baldock C, Weiss AS, Buehler MJ. Molecular model of human tropoelastin and implications of associated mutations. Proceedings of the National Academy of Sciences 2018;115:7338-43.
[2] Yeo GC, Tarakanova A, Baldock C, Wise SG, Buehler MJ, Weiss AS. Subtle balance of tropoelastin molecular shape and flexibility regulates dynamics and hierarchical assembly. Science Advances 2016;2:e1501145.
[3] Vrhovski B, Weiss AS. Biochemistry of tropoelastin. European Journal of Biochemistry 1998;258:1-18.
[4] Mercedes S, Constancio G-O, Doriana O, Eduardo Perez del R, Francisco JA. Advanced Systems for Controlled Drug Delivery from Chemically Modified Elastin-like Recombinamers. Current Organic Chemistry 2017;21:21-33.
[5] Baul U, Bley M, Dzubiella J. Thermal Compaction of Disordered and Elastin-like Polypeptides: A Temperature-Dependent, Sequence-Specific Coarse-Grained Simulation Model. Biomacromolecules 2020;21:3523-38.
[6] Quintanilla-Sierra L, Garcia-Arevalo C, Rodriguez-Cabello JC. Self-assembly in elastin-like recombinamers: a mechanism to mimic natural complexity. Materials today Bio 2019;2:100007.
[7] Zhao B, Li NK, Yingling YG, Hall CK. LCST Behavior is Manifested in a Single Molecule: Elastin-Like polypeptide (VPGVG)n. Biomacromolecules 2016;17:111-8.
[8] Li NK, Roberts S, Quiroz FG, Chilkoti A, Yingling YG. Sequence Directionality Dramatically Affects LCST Behavior of Elastin-Like Polypeptides. Biomacromolecules 2018;19:2496-505.
[9] Li NK, Quiroz FG, Hall CK, Chilkoti A, Yingling YG. Molecular Description of the LCST Behavior of an Elastin-Like Polypeptide. Biomacromolecules 2014;15:3522-30.
[10] Prhashanna A, Taylor PA, Qin J, Kiick KL, Jayaraman A. Effect of Peptide Sequence on the LCST-Like Transition of Elastin-Like Peptides and Elastin-Like Peptide–Collagen-Like Peptide Conjugates: Simulations and Experiments. Biomacromolecules 2019;20:1178-89.
[11] Urry DW, Starcher B, Partridge SM. Coacervation of Solubilized Elastin effects a Notable Conformational Change. Nature 1969;222:795-6.
[12] Roberts S, Dzuricky M, Chilkoti A. Elastin-like polypeptides as models of intrinsically disordered proteins. FEBS Letters 2015;589:2477-86.
[13] Ruff KM, Roberts S, Chilkoti A, Pappu RV. Advances in Understanding Stimulus-Responsive Phase Behavior of Intrinsically Disordered Protein Polymers. Journal of Molecular Biology 2018;430:4619-35.
[14] Rauscher S, Baud S, Miao M, Keeley Fred W, Pomès R. Proline and Glycine Control Protein Self-Organization into Elastomeric or Amyloid Fibrils. Structure 2006;14:1667-76.
[15] Muiznieks LD, Keeley FW. Proline Periodicity Modulates the Self-assembly Properties of Elastin-like Polypeptides. Journal of Biological Chemistry 2010;285:39779-89.
[16] McDaniel JR, Radford DC, Chilkoti A. A Unified Model for De Novo Design of Elastin-like Polypeptides with Tunable Inverse Transition Temperatures. Biomacromolecules 2013;14:2866-72.
[17] Tarakanova A, Huang W, Weiss AS, Kaplan DL, Buehler MJ. Computational smart polymer design based on elastin protein mutability. Biomaterials 2017;127:49-60.

[18] Prhashanna A, Taylor PA, Qin J, Kiick KL, Jayaraman A. Effect of Peptide Sequence on the LCST-Like Transition of Elastin-Like Peptides and Elastin-Like Peptide-Collagen-Like Peptide Conjugates: Simulations and Experiments. Biomacromolecules 2019;20:1178-89.
[19] Cho Y, Zhang Y, Christensen T, Sagle LB, Chilkoti A, Cremer PS. Effects of Hofmeister Anions on the Phase Transition Temperature of Elastin-like Polypeptides. The Journal of Physical Chemistry B 2008;112:13765-71.
[20] Pinedo-Martín G, Santos M, Testera AM, Alonso M, Rodríguez-Cabello JC. The effect of NaCl on the self-assembly of elastin-like block co-recombinamers: Tuning the size of micelles and vesicles. Polymer 2014;55:5314-21.
[21] Pinedo-Martín G, Castro E, Martín L, Alonso M, Rodríguez-Cabello JC. Effect of Surfactants on the Self-Assembly of a Model Elastin-like Block Corecombinamer: From Micelles to an Aqueous Two-Phase System. Langmuir 2014;30:3432-40.
[22] Mackay JA, Callahan DJ, Fitzgerald KN, Chilkoti A. Quantitative model of the phase behavior of recombinant pH-responsive elastin-like polypeptides. Biomacromolecules 2010;11:2873-9.
[23] Meyer DE, Chilkoti A. Quantification of the Effects of Chain Length and Concentration on the Thermal Behavior of Elastin-like Polypeptides. Biomacromolecules 2004;5:846-51.
[24] Ribeiro A, Arias FJ, Reguera J, Alonso M, Rodríguez-Cabello JC. Influence of the Amino-Acid Sequence on the Inverse Temperature Transition of Elastin-Like Polymers. Biophysical Journal 2009;97:312-20.
[25] Widder K, MacEwan SR, Garanger E, Núñez V, Lecommandoux S, Chilkoti A, Hinderberger D. Characterisation of hydration and nanophase separation during the temperature response in hydrophobic/hydrophilic elastin-like polypeptide (ELP) diblock copolymers. Soft Matter 2017;13:1816-22.
[26] Christensen T, Hassouneh W, Trabbic-Carlson K, Chilkoti A. Predicting Transition Temperatures of Elastin-Like Polypeptide Fusion Proteins. Biomacromolecules 2013;14:1514-9.
[27] Xia X-X, Xu Q, Hu X, Qin G, Kaplan DL. Tunable Self-Assembly of Genetically Engineered Silk–Elastin-like Protein Polymers. Biomacromolecules 2011;12:3844-50.
[28] Fernández-Colino A, Arias FJ, Alonso M, Rodríguez-Cabello JC. Self-Organized ECM-Mimetic Model Based on an Amphiphilic Multiblock Silk-Elastin-Like Corecombinamer with a Concomitant Dual Physical Gelation Process. Biomacromolecules 2014;15:3781-93.
[29] Guo C, Li C, Kaplan DL. Enzymatic Degradation of Bombyx mori Silk Materials: A Review. Biomacromolecules 2020;21:1678-86.
[30] Asakura T, Yao J. 13C CP/MAS NMR study on structural heterogeneity in Bombyx mori silk fiber and their generation by stretching. Protein science : a publication of the Protein Society 2002;11:2706-13.
[31] Sirichaisit J, Brookes VL, Young RJ, Vollrath F. Analysis of Structure/Property Relationships in Silkworm (Bombyx mori) and Spider Dragline (Nephila edulis) Silks Using Raman Spectroscopy. Biomacromolecules 2003;4:387-94.
[32] Hu X, Wang X, Rnjak J, Weiss AS, Kaplan DL. Biomaterials derived from silk-tropoelastin protein systems. Biomaterials 2010;31:8121-31.
[33] Ha S-W, Tonelli AE, Hudson SM. Structural Studies of Bombyx mori Silk Fibroin during Regeneration from Solutions and Wet Fiber Spinning. Biomacromolecules 2005;6:1722-31.
[34] Cebe P, Partlow BP, Kaplan DL, Wurm A, Zhuravlev E, Schick C. Silk I and Silk II studied by fast scanning calorimetry. Acta Biomaterialia 2017;55:323-32.
[35] Keten S, Xu Z, Ihle B, Buehler MJ. Nanoconfinement controls stiffness, strength and mechanical toughness of [beta]-sheet crystals in silk. Nat Mater 2010;9:359-67.
[36] Drummy LF, Farmer BL, Naik RR. Correlation of the β-sheet crystal size in silk fibers with the protein amino acid sequence. Soft Matter 2007;3:877-82.
[37] Fernández-Colino A, Arias FJ, Alonso M, Rodríguez-Cabello JC. Amphiphilic Elastin-Like Block Co-Recombinamers Containing Leucine Zippers: Cooperative Interplay between Both Domains Results in Injectable and Stable Hydrogels. Biomacromolecules 2015;16:3389-98.

[38] Xia X-X, Wang M, Lin Y, Xu Q, Kaplan DL. Hydrophobic Drug-Triggered Self-Assembly of Nanoparticles from Silk-Elastin-Like Protein Polymers for Drug Delivery. Biomacromolecules 2014;15:908-14.
[39] Roberts EG, Rim N-G, Huang W, Tarakanova A, Yeo J, Buehler MJ, Kaplan DL, Wong JY. Fabrication and Characterization of Recombinant Silk-Elastin-Like-Protein (SELP) Fiber. Macromolecular Bioscience 2018;18:1800265.
[40] Yeo J, Huang W, Tarakanova A, Zhang Y-W, Kaplan DL, Buehler MJ. Unraveling the molecular mechanisms of thermo-responsive properties of silk-elastin-like proteins by integrating multiscale modeling and experiment. Journal of Materials Chemistry B 2018;6:3727-34.
[41] Huang W, Tarakanova A, Dinjaski N, Wang Q, Xia X, Chen Y, Wong JY, Buehler MJ, Kaplan DL. Design of Multistimuli Responsive Hydrogels Using Integrated Modeling and Genetically Engineered Silk–Elastin-Like Proteins. Advanced Functional Materials 2016;26:4113-23.
[42] Valiaev A, Lim DW, Schmidler S, Clark RL, Chilkoti A, Zauscher S. Hydration and Conformational Mechanics of Single, End-Tethered Elastin-like Polypeptides. Journal of the American Chemical Society 2008;130:10939-46.
[43] Valiaev A, Lim DW, Oas TG, Chilkoti A, Zauscher S. Force-Induced Prolyl Cis−Trans Isomerization in Elastin-like Polypeptides. Journal of the American Chemical Society 2007;129:6491-7.
[44] Cipriani F, Krüger M, de Torre IG, Sierra LQ, Rodrigo MA, Kock L, Rodriguez-Cabello JC. Cartilage Regeneration in Preannealed Silk Elastin-Like Co-Recombinamers Injectable Hydrogel Embedded with Mature Chondrocytes in an Ex Vivo Culture Platform. Biomacromolecules 2018;19:4333-47.
[45] Ibáñez-Fonseca A, Orbanic D, Arias FJ, Alonso M, Zeugolis DI, Rodríguez-Cabello JC. Influence of the Thermodynamic and Kinetic Control of Self-Assembly on the Microstructure Evolution of Silk-Elastin-Like Recombinamer Hydrogels. Small 2020;16:2001244.
[46] Dandu R, Cresce AV, Briber R, Dowell P, Cappello J, Ghandehari H. Silk–elastinlike protein polymer hydrogels: Influence of monomer sequence on physicochemical properties. Polymer 2009;50:366-74.
[47] Cole MA, Voelcker NH, Thissen H, Griesser HJ. Stimuli-responsive interfaces and systems for the control of protein–surface and cell–surface interactions. Biomaterials 2009;30:1827-50.
[48] Ding X, Li G, Zhang P, Xiao C. Constructing Thermally Reversible Dynamic Hydrogels via Catalysis-Free Knoevenagel Condensation. ACS Macro Letters 2020;9:830-5.
[49] Rosales AM, Anseth KS. The design of reversible hydrogels to capture extracellular matrix dynamics. Nature Reviews Materials 2016;1:15012.
[50] Narayan OP, Mu X, Hasturk O, Kaplan DL. Dynamically tunable light responsive silk-elastin-like proteins. Acta Biomaterialia 2021;121:214-23.
[51] Parker RN, Cairns DM, Wu WA, Jordan K, Guo C, Huang W, Martin-Moldes Z, Kaplan DL. Smart Material Hydrogel Transfer Devices Fabricated with Stimuli-Responsive Silk-Elastin-Like Proteins. Advanced Healthcare Materials 2020;9:2000266.
[52] González-Obeso C, González-Pérez M, Mano JF, Alonso M, Rodríguez-Cabello JC. Complex Morphogenesis by a Model Intrinsically Disordered Protein. Small 2020;16:2005191.
[53] Gonzalez-Obeso C, Girotti A, Rodriguez-Cabello JC. A transferrin receptor-binding mucoadhesive elastin-like recombinamer: In vitro and in vivo characterization. Acta Biomater 2019;88:241-50.
[54] Hu X, Kaplan D, Cebe P. Determining Beta-Sheet Crystallinity in Fibrous Proteins by Thermal Analysis and Infrared Spectroscopy. Macromolecules 2006;39:6161-70.
[55] Teng W, Cappello J, Wu X. Recombinant Silk-Elastinlike Protein Polymer Displays Elasticity Comparable to Elastin. Biomacromolecules 2009;10:3028-36.
[56] Qiu W, Teng W, Cappello J, Wu X. Wet-spinning of recombinant silk-elastin-like protein polymer fibers with high tensile strength and high deformability. Biomacromolecules 2009;10:602-8.

[57] Teng W, Cappello J, Wu X. Physical crosslinking modulates sustained drug release from recombinant silk-elastinlike protein polymer for ophthalmic applications. Journal of Controlled Release 2011;156:186-94.
[58] Teng W, Huang Y, Cappello J, Wu X. Optically Transparent Recombinant Silk-Elastinlike Protein Polymer Films. The Journal of Physical Chemistry B 2011;115:1608-15.
[59] Schmidt P, Dybal Jí, Rodríguez-Cabello JC, Alonso M. Raman spectroscopy of secondary structure of elastinlike polymer poly(GVGVP). Biopolymers 2001;62:150-7.
[60] Wang L, Lu C, Zhang B, Zhao B, Wu F, Guan S. Fabrication and characterization of flexible silk fibroin films reinforced with graphene oxide for biomedical applications. RSC Advances 2014;4:40312-20.
[61] Lu S, Li J, Zhang S, Yin Z, Xing T, Kaplan DL. The influence of the hydrophilic-lipophilic environment on the structure of silk fibroin protein. Journal of Materials Chemistry B 2015;3:2599-606.
[62] Li M, Ogiso M, Minoura N. Enzymatic degradation behavior of porous silk fibroin sheets. Biomaterials 2003;24:357-65.
[63] Acosta S, Quintanilla-Sierra L, Mbundi L, Reboto V, Rodríguez-Cabello JC. Elastin-Like Recombinamers: Deconstructing and Recapitulating the Functionality of Extracellular Matrix Proteins Using Recombinant Protein Polymers. Advanced Functional Materials 2020;30:1909050.
[64] Kim W, Chaikof EL. Recombinant elastin-mimetic biomaterials: Emerging applications in medicine. Advanced Drug Delivery Reviews 2010;62:1468-78.
[65] Wright ER, Conticello VP. Self-assembly of block copolymers derived from elastin-mimetic polypeptide sequences. Adv Drug Deliv Rev 2002;54:1057-73.
[66] Jiang T, Zukoski CF. Role of Particle Size and Polymer Length in Rheology of Colloid–Polymer Composites. Macromolecules 2012;45:9791-803.
[67] Guan Y, You H, Cai J, Zhang Q, Yan S, You R. Physically crosslinked silk fibroin/hyaluronic acid scaffolds. Carbohydrate Polymers 2020;239:116232.
[68] Dhandhukia JP, Brill DA, Kouhi A, Pastuszka MK, MacKay JA. Elastin-like polypeptide switches: A design strategy to detect multimeric proteins. Protein Science 2017;26:1785-95.
[69] Meyer DE, Kong GA, Dewhirst MW, Zalutsky MR, Chilkoti A. Targeting a genetically engineered elastin-like polypeptide to solid tumors by local hyperthermia. Cancer Res 2001;61:1548-54.
[70] Monti P, Freddi G, Bertoluzza A, Kasai N, Tsukada M. Raman spectroscopic studies of silk fibroin from Bombyx mori. Journal of Raman Spectroscopy 1998;29:297-304.
[71] Wang H-Y, Zhang Y-Q. Processing and characterisation of a novel electropolymerized silk fibroin hydrogel membrane. Scientific Reports 2014;4:6182.
[72] Zhang F, Lu Q, Ming J, Dou H, Liu Z, Zuo B, Qin M, Li F, Kaplan DL, Zhang X. Silk dissolution and regeneration at the nanofibril scale. Journal of Materials Chemistry B 2014;2:3879-85.
[73] Guo C, Li C, Vu HV, Hanna P, Lechtig A, Qiu Y, Mu X, Ling S, Nazarian A, Lin SJ, Kaplan DL. Thermoplastic moulding of regenerated silk. Nature Materials 2020;19:102-8.
[74] Guo C, Zhang J, Wang X, Nguyen AT, Liu XY, Kaplan DL. Comparative Study of Strain-Dependent Structural Changes of Silkworm Silks: Insight into the Structural Origin of Strain-Stiffening. Small 2017;13:1702266.
[75] Somashekar R, Gopalkrishne Urs R. Simulation of X-ray diffraction patterns for silk fibres using paracrystalline statistics. Pramana 1993;40:335-43.
[76] Stokes AR, Wilson AJC. The diffraction of X rays by distorted crystal aggregates - I. Proceedings of the Physical Society 1944;56:174-81.
[77] Wilson A. The diffraction of x-rays by distorted-crystal aggregates. II. Diffraction by bent lamellae. Acta Crystallographica 1949;2:220-2.
[78] Eastabrook JN, Wilson AJC. The Diffraction of X-Rays by Distorted-Crystal Aggregates III: Remarks on the Interpretation of the Fourier Coefficients. Proceedings of the Physical Society Section B 1952;65:67-75.

[79] Somashekar R, Urs RG, Madhava MS. Crystal size and distortion parameter of natural pure mysore silk fibers (Bombyx Mori). Journal of Applied Polymer Science 1992;44:2161-5.
[80] Urry DW, Gowda DC, Parker TM, Luan C-H, Reid MC, Harris CM, Pattanaik A, Harris RD. Hydrophobicity scale for proteins based on inverse temperature transitions. Biopolymers 1992;32:1243-50.
[81] Varanko AK, Su JC, Chilkoti A. Elastin-Like Polypeptides for Biomedical Applications. Annual Review of Biomedical Engineering 2020;22:343-69.
[82] Tarakanova A, Huang W, Qin Z, Kaplan DL, Buehler MJ. Modeling and Experiment Reveal Structure and Nanomechanics across the Inverse Temperature Transition in B. mori Silk-Elastin-like Protein Polymers. ACS Biomaterials Science & Engineering 2017;3:2889-99.
[83] Martín L, Arias FJ, Alonso M, García-Arévalo C, Rodríguez-Cabello JC. Rapid micropatterning by temperature-triggered reversible gelation of a recombinant smart elastin-like tetrablock-copolymer. Soft Matter 2010;6:1121-4.
[84] Baldock C, Oberhauser AF, Ma L, Lammie D, Siegler V, Mithieux SM, Tu Y, Chow JYH, Suleman F, Malfois M, Rogers S, Guo L, Irving TC, Wess TJ, Weiss AS. Shape of tropoelastin, the highly extensible protein that controls human tissue elasticity. Proceedings of the National Academy of Sciences 2011;108:4322.
[85] Urry DW, Hugel T, Seitz M, Gaub HE, Sheiba L, Dea J, Xu J, Parker T. Elastin: a representative ideal protein elastomer. Philos Trans R Soc Lond B Biol Sci 2002;357:169-84.
[86] Stock P, Monroe JI, Utzig T, Smith DJ, Shell MS, Valtiner M. Unraveling Hydrophobic Interactions at the Molecular Scale Using Force Spectroscopy and Molecular Dynamics Simulations. ACS Nano 2017;11:2586-97.
[87] Li B, Alonso DOV, Bennion BJ, Daggett V. Hydrophobic Hydration Is an Important Source of Elasticity in Elastin-Based Biopolymers. Journal of the American Chemical Society 2001;123:11991-8.
[88] Xiao S, Xiao S, Gräter F. Dissecting the structural determinants for the difference in mechanical stability of silk and amyloid beta-sheet stacks. Physical Chemistry Chemical Physics 2013;15:8765-71.
[89] Liu R, Deng Q, Yang Z, Yang D, Han M-Y, Liu XY. “Nano-Fishnet” Structure Making Silk Fibers Tougher. Advanced Functional Materials 2016;26:5534-41.
[90] Cheng Y, Koh L-D, Li D, Ji B, Han M-Y, Zhang Y-W. On the strength of β-sheet crystallites of Bombyx mori silk fibroin. Journal of The Royal Society Interface 2014;11:20140305.